The Endocochlear Potential Alters Cochlear Micromechanics

Stefan Jacob,[†] Martin Pienkowski,[†‡] and Anders Fridberger[†§*]

[†]Center for Hearing and Communication Research, Karolinska Institutet, Departments of Clinical Neuroscience and Otolaryngology, M1 Karolinska University Hospital, Stockholm, Sweden; [‡]Departments of Physiology and Pharmacology, and Department of Psychology, University of Calgary, Calgary, Alberta, Canada; and [§]Oregon Hearing Research Center, Oregon Health & Science University, Portland, Oregon

ABSTRACT Acoustic stimulation gates mechanically sensitive ion channels in cochlear sensory hair cells. Even in the absence of sound, a fraction of these channels remains open, forming a conductance between hair cells and the adjacent fluid space, scala media. Restoring the lost endogenous polarization of scala media in an in vitro preparation of the whole cochlea depolarizes the hair cell soma. Using both digital laser interferometry and time-resolved confocal imaging, we show that this causes a structural refinement within the organ of Corti that is dependent on the somatic electromotility of the outer hair cells (OHCs). Specifically, the inner part of the reticular lamina up to the second row of OHCs is pulled toward the basilar membrane, whereas the outer part (third row of OHCs and the Hensen's cells) unexpectedly moves in the opposite direction. A similar differentiated response pattern is observed for sound-evoked vibrations: restoration of the endogenous polarization decreases vibrations of the inner part of the reticular lamina and results in up to a 10-fold increase of vibrations of the outer part. We conclude that the endogenous polarization of scala media affects the function of the hearing organ by altering its geometry, mechanical and electrical properties.

INTRODUCTION

The sensory hair cells in the organ of Corti are equipped with hair bundles that vibrate during acoustic stimulation, thereby activating mechanoelectric transducer (MET) channels (1–3). To signal both excitatory and inhibitory bundle deflections, a fraction of the MET channels stays open at rest (4). Thus, even in the absence of sound, a standing silent current may enter the hair cells (5,6). This current depolarizes the inner hair cells that transduce acoustic vibrations into neural impulses (7,8). Outer hair cells (OHC), on the other hand, react to electrical polarization changes by actively generating hair bundle movement (9), and by altering cell length (10,11) and stiffness (12). The latter two effects arise from somatic electromotility, which is associated with prestin (13), a protein in the OHC basolateral membrane (14,15). Existing data suggest that changes to the so-called endocochlear potential (EP), the endogenous polarization of scala media, which drives the transduction current, may lead to static deformations of the hearing organ (16–20). Thus, the internal geometry and mechanical properties of the hearing organ, both of which are crucial for sound encoding, can be modified (21,22). Using digital laser interferometry (23) and time-resolved confocal imaging (24,25), this study investigates how the static endogenous polarization of scala media influences both the structure and the micromechanics of the intact hearing organ, in an in vitro preparation of the guinea pig temporal bone.

We hypothesized that restoration of the positive endogenous EP, achieved by quasistatic current injections into scala media, would lead to a continuous depolarization of the OHCs, triggering a series of structural modifications within the organ of Corti, and increasing the amplitude of sound-evoked vibrations. We show that restoring the EP induced sustained deformations of the hearing organ that proved more complex than expected. Furthermore, restoring the EP does indeed modulate the vibrations of the reticular lamina, thus supplying evidence that apical-turn OHCs do in fact amplify sound, which has been a long-standing point of contention (26–28). We also show that both static and dynamic mechanical consequences of EP restoration depend on the somatic electromotility of OHCs. We conclude that the positive endogenous EP prepares the hearing organ for optimal sound reception by fine-tuning its geometry and mechanoelectrical properties.

MATERIALS AND METHODS

Animal preparation

All animal procedures were approved by the local ethics committee (permit N319/06). Young guinea pigs were anesthetized, decapitated, and the temporal bone quickly removed and attached in a custom-made holder allowing natural stimulation of the eardrum with sound. The bulla was opened, exposing the middle ear, and the preparation was submerged in tissue culture medium (Minimum Essential Medium, Invitrogen, Carlsbad, CA). A small opening, a triangle the size of ~0.35 mm^2, was made in the apex of the cochlea, and an electrode advanced into scala media penetrating the otherwise intact Reissner's membrane (see Fig. S1 in the Supporting Material). Scala tympani was continuously perfused with oxygenated medium (~0.6 ml/h); the perfusion system also served as a route for drug delivery to the hair cells. Perfusion may cause static position shifts of the organ of Corti. Control experiments, lacking perfusion, showed no observable difference in cochlear vibration patterns, but both the endogenous EP and the general physiological condition of these preparations decayed more

Submitted January 26, 2011, and accepted for publication May 3, 2011.

*Correspondence: anders.fridberger@ki.se

Editor: Andrew McCulloch.

0006-3495/11/06/2586/9 $2.00

doi: 10.1016/j.bpj.2011.05.002

rapidly (see below). All experiments were carried out at room temperature (~21°C).

Typically, at the beginning of the data acquisition (~25 min after decapitation), the endogenous EP in scala media was still relatively high, in the range of +15 to +50 mV (in vivo: +60 mV (29)). The EP steadily decays toward 0 mV during the experiment (30), and levels off at around 0 mV about 1 h after decapitation. Reoxygenation of cochlear tissues within 10 min of decapitation (via the perfusion medium) was responsible for the range of positive EPs observed at the beginning of our experiments (31,32). In the absence of perfusion, the starting EP was measured to be negative. Perfused preparations with an EP of < -10 mV at the time of electrode penetration, indicating surgical damage, were discarded. Data collection was also aborted if the cochlear microphonic potentials, measured repeatedly throughout the experiment, underwent sudden changes. Current-evoked motions were also used as an indicator of preparation quality. If no such motion could be evoked or the amplitude of the motion suddenly decreased, the preparation was discarded.

Interferometry

A custom interferometer (23) with a 25× lens (33) and noise floor of < 15 pm/$\sqrt{\text{Hz}}$ was used for measuring organ of Corti motion. Artificial reflectors were not required. The preparation was oriented with the basilar membrane nearly perpendicular to the optical axis. To measure the angle of the preparation and check preparation condition, hair cells were visualized with confocal microscopy at the end of the interferometry experiments, after staining with RH-795 (5 μM, Biotium, Howard, CA). Data were averaged 10 times and were not corrected for any projection effect arising from the angle of the preparation, as this factor and its variance was quite small. To avoid charge buildup in scala media, two different protocols were used for current injection. The first protocol generates a positive current pulse in the second quarter (50–100 ms) of the measurement window (0–200 ms) and a negative current pulse in the third quarter (100–150 ms) of the window. In the second protocol, the current pulse under investigation was placed in the second and third quarter (50–150 ms) of the measurement window (0–200 ms) (Fig. 1 *A*), whereas the charge balancing pulse was located outside (300–400 ms) of the measurement window. There was no systematic difference in the cochlear response to the two stimulation protocols.

Time-resolved confocal imaging

Measurements were performed on a Zeiss LSM 510 laser scanning confocal microscope, using a 40× lens. Hair cells were stained with 5 μM RH-795, delivered through the perfusion system (34). It was important to limit laser excitation to prevent cellular damage ($P_{ex} < 30$ μW, typical $P_{ex} \leq 18$ μW). Therefore, image resolution was sacrificed for an acceptable signal/noise ratio (Fig. 2 *A*). To avoid charge buildup in scala media, the current injection switched directly from positive to negative at 5 Hz. Because this frequency is 4–5 octaves below the sound stimulus, the current injection is considered static. Image acquisition triggered stimulus presentation, as detailed previously (25). Briefly, each measurement consisted of a time series of 37 images. The time of acquisition for a given pixel corresponds to a known phase of the acoustic stimulus (sinusoid) and a known phase of the current injection (square wave). The phase of the current stimulus mapped to three possible outcomes: positive current for (pi/3,pi), negative current for (4*pi/3,2*pi), and two transition phases that were discarded. The intensity in each pixel was sampled uniformly in the whole phase plane, with the acoustic stimulus phase divided into 12 bins, and current injection into 3 bins, assuming periodicity of the pixel intensity along both axes. Still images at a given current and acoustic stimulus phase were then reconstructed as described previously (25). Reconstructed images were low-pass filtered and an optical flow computation performed (35). The position shift was estimated by optical flow computations between images during positive and the negative current at the same acoustic phase, followed by averaging over the acoustic phases. Note that our one-photon confocal microscope could not image the basal half of the OHCs.

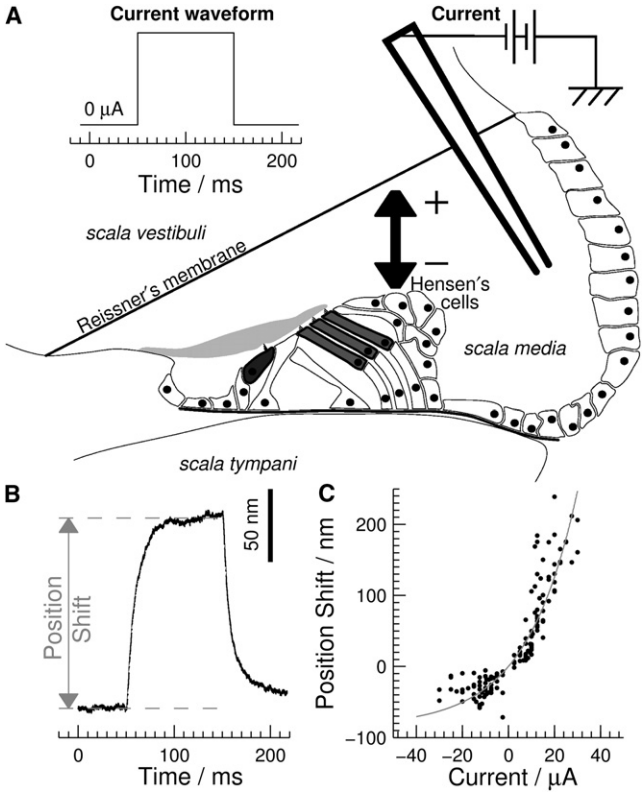

FIGURE 1 (*A*) Schematic cross section of the cochlea with the three rows of outer hair cells colored light gray and one row of inner hair cells colored dark gray. The preparation was stimulated with sound and electrical current (*inset*). Bold arrow indicates measurement site of interferometry experiments on the reticular lamina and illustrates the polarity of the position shift. (*B*) Interferometer measurement of Hensen's cell motion during direct current (+10 μA) stimulation. (*C*) Position shift amplitude as a function of applied direct current (x); data were pooled from nine experiments at comparable experimental time points. Data were fitted to a reduced exponential function: $F[x] = c_1\exp[c_2x] - c_1$, where $c_1 = 84.1$ nm, $c_2 = 0.05$ μA^{-1}.

Electrophysiology

Borosilicate glass microelectrodes were used for the measurements of cochlear potentials and for drug injections. To inject drugs from the electrode while preserving the ionic composition in scala media, an endolymph-like filling solution was used (1.3 mM NaCl, 31 mM $KHCO_3$, 23 μM $CaCl_2$, 128.3 mM KCl; pH = 7.4; 300 mOsm). Electrodes were beveled to 2 MΩ. FM1-43 (50 μM, Invitrogen) or d-tubocurarine (50 μM, Sigma-Aldrich, St. Louis, MO) were dissolved in the filling solution and injected through electrophoresis. Control measurements without pharmaceuticals in the electrodes showed that electrophoresis caused no damage, as there was no change in cochlear microphonic potentials, sound-evoked motion, or hair cell morphology. Electrode potentials were sampled with either a 16-bit A/D board (National Instruments, Austin, TX) or a signal analyzer (35665A, Hewlett Packard, Palo Alto, CA), after appropriate amplification (IX1, Dragan, Minneapolis, MN; equipped with 10× head stage). The current injection was performed with a linear stimulus isolator (A395, WPI, Sarasota, FL) driven by custom software.

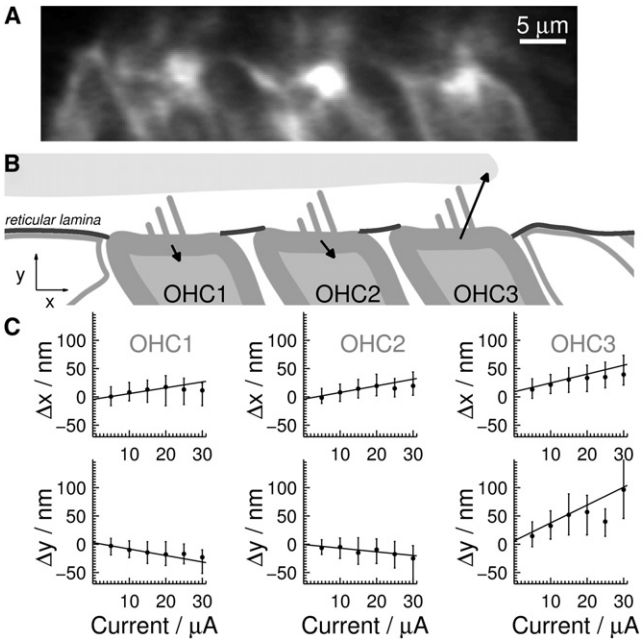

FIGURE 2 Position shift of the reticular lamina; microscopy measurements. (*A*) Image from the extracted image series showing the top of the three rows of OHCs during current and sound stimulation. Note RH 795 does not stain the tectorial membrane. (*B*) Schematic of 2*A*; arrows illustrate the position shift of the OHC apex when switching from -30 μA to $+30$ μA. Arrows are 50× magnified relative to the anatomical scale. (*C*) Average position shift of the OHC apex when switching from negative to positive current as a function of current magnitude. Error bars indicate 25% and 75% quartile. Coordinate system is illustrated in *B*. Position shift amplitudes were fitted to a linear model (*solid lines*) for currents between 5 and 20 μA; larger currents affected most preparations negatively.

Statistics

The dependent variable, e.g., position shift amplitude, was modeled via linear regression and nonlinear behavior was linearized by a reduced exponential transform of the dependent variable. The transform parameter was obtained from the reduced exponential fit (see Fig. 1 *C*) and held constant for further analysis. After careful examination of the residuals an analysis of variance was performed on the model to access statistical significance (36). The analysis of variance was controlled for the unbalanced independent variable, e.g., current amplitude.

RESULTS

Static position shift

Current injections can change the electrical polarization of scala media with respect to the perilymph, such that positive current leads to positive polarization. During 50- or 100-ms-long current steps, the apical (i.e., scala media facing) surface of the Hensen's cells moved to a new position. Positive current injections displaced the surface toward scala vestibuli (Fig. 1 *B*; *upward* in Fig. 1 *A*, *bold arrow* marks measurement site), whereas negative current displaced it toward scala tympani. The position shift displayed fast onsets and offsets (Fig. 1 *B*) and was fully reversible for currents up to 30 μA. This particular response polarity was observed in all 28 preparations (shorthand, $N_{prep} = 28$) and was unexpected as positive polarization of scala media is believed to depolarize the soma of the hair cells, which results in contraction of isolated OHCs (11). Thus, restoring the EP was expected to shift the Hensen's cells in the opposite direction, toward scala tympani.

The functional relation between the size of the current step and the position shift amplitude is nonlinear (Fig. 1 *C*).The data presented in this plot were obtained from nine different preparations, more than 1 h after decapitation to make sure that the endogenous EP had decayed to zero. Position shifts reached their lower limit, about -40 nm, for currents below -4 μA, but did not reach their upper limit, >200 nm, due to experimental constraints in injecting currents larger than 30 μA. A reduced exponential function produced a satisfactory fit of the experimental data (Fig. 1 *C*) and an analysis of variance, controlling for the current, demonstrated that the relation between current and position shift was significant ($p < 0.001$). Measurements in proximity to the electrode and up to 300 μm away, a range limited by the size of the apical cochlear opening, showed similar position shifts. This indicates that the current injection had a large spatial extent and that the generated potential was at least locally comparable to the uniform EP found in vivo. From these data, it is clear that the resting position of the organ of Corti depends on the size and sign of the EP.

Structural modifications

Imaging can detect the complex multidimensional motion that occurs in the cochlea (18,19,37,38). Therefore, time-resolved confocal imaging was used to investigate the unexpected polarity of the position shift in more detail. The imaging method constrained the waveform of the current stimulus to be a square wave, in this case switching directly from positive to negative current and back. The data revealed that the apical surfaces of the individual OHC rows responded differently to current injections (Fig. 2 *B*; $N_{prep} = 24$). When switching from negative to positive current, the position shift amplitude was almost equal for OHC row one and two, but more than twice as large for OHC row three. The average position shift component parallel to the reticular lamina (*x*-component) increased with increasing current levels and was similar for all three rows of OHCs (Fig. 2 *C*; *top panels*). The relation between current size and the *x*-component was not significantly different between the OHC rows. The position shift component perpendicular to the reticular lamina (*y*-component) was significantly different between the first two OHC rows and the third row (Fig. 2 *C*; *bottom panels*; $p < 0.001$). The *y*-component was positive for OHC row three, indicating a shift toward scala vestibuli, and negative for OHC row one and two, indicating a shift toward scala tympani. Note that the amplitude and direction of the

OHC row three position shifts was consistent with the interferometric measurements from the Hensen's cells, which are closest to OHC row three.

The confocal imaging experiments showed an almost linear relation between the size of the injected current and the position shift amplitude, whereas the interferometry data showed an exponential relation. This contradiction can be readily resolved by considering the reference points, from which the position shift is calculated. The reference point in the interferometer setup is the cochlear position at zero current, although in the microscopy setup it is the position during negative current injection. Hence, the exponentially saturating position shift from zero current to the microscopy reference point partially compensates the exponential growth of the position shift during positive current injections (Fig. 1 *C*).

Fig. 3 *A* shows raw imaging data of an OHC3 soma during quasistatic current injections into scala media, as indicated by the white bars on the right side of the image. The soma of the OHC3 moved toward the Hensen's cells when the current injection switched from negative to positive (Fig. 3 *B*; Fig. S2 in the Supporting Material). The part of the position shift perpendicular to the lateral cell membrane became significantly larger with increasing distance from the apex of the cell ($p < 0.001$). This can already be seen in the raw data, because thick block-like features, which indicate motion, become larger toward the bottom of the image (Fig. 3 *A*). For the apical half of OHC row three the perpendicular component was analyzed by a linear regression of the pooled data, as illustrated in Fig. 3 *B*. The slope of the linear fit increased with current level and slowly saturated for larger currents (Fig. 3 *C*). A similar tendency could be seen for the intercept of the fit (Fig. 3 *D*). This means that at the saturating current, the lateral wall will undergo an average position shift that increases almost 6 nm/μm distance from the apex of the cell.

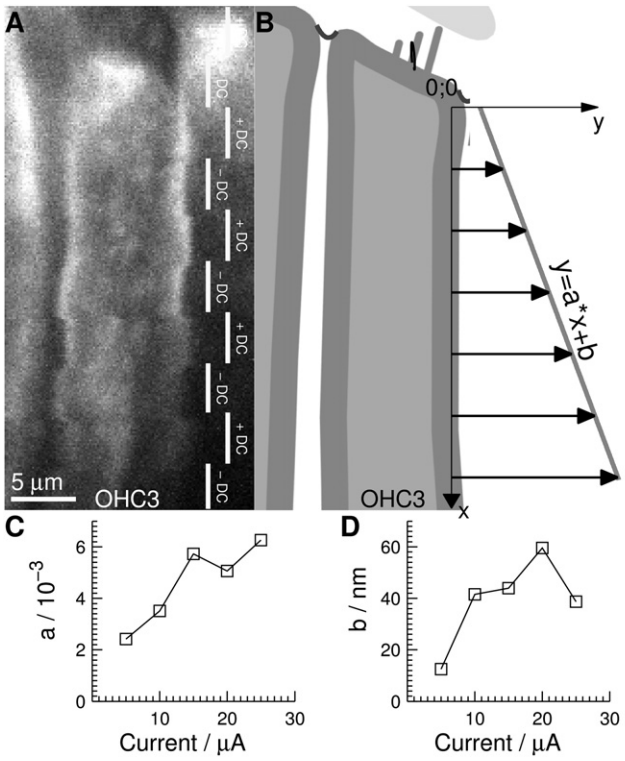

FIGURE 3 Position shift of the OHC row three soma; microscopy measurements. (*A*) Raw, unprocessed confocal image showing OHC row three soma during sound and current stimulation. The injected current, illustrated by the white bars, causes the thick block-like features that indicate motion. (*B*) Schematic of *A*; arrows illustrate the averaged position shift (y) of the lateral cell membrane of OHC row three when switching from -25 μA to $+25$ μA. The position shift (y) is fitted to a linear function of the distance from the reticular lamina (x). Arrows are 50× magnified. The trajectory, 50× magnified, at top of the OHC shows the displacement of the cuticular plate during one period of sound (150 Hz, 84 dB SPL) and illustrates the size of the position shift. (*C* and *D*) Slope and intercept of the linear fit of the pooled data from the OHC lateral cell membrane position shift when switching from negative to positive current.

OHC polarization

In the confocal imaging experiments, it was also possible to test the underlying assumption that positive current injection into scala media depolarizes the OHC lateral membrane. To do so, we analyzed the fluorescence intensity changes of the voltage-sensitive dye RH-795, which stained the OHC lateral membrane, but did not reach the hair bundles when administered through the perfusion system. The fluorescence intensity increased during negative current injections, and decreased during positive current injections, showing that positive current depolarized the OHC soma. Furthermore, a decrease in fluorescence intensity was also observed during perfusion of scala tympani with isomolar tissue culture medium containing 50 mM KCl. It was previously shown that a substantial potassium concentration in scala tympani depolarizes hair cells (39). This demonstrates that positive current injection into scala media depolarizes the OHC lateral membrane whereas negative current hyperpolarizes it.

Sound-evoked vibrations

To study if the quasistatic current injections into scala media have an immediate effect on the sound-induced vibrations, we stimulated the hearing organ simultaneously with current steps and sound in the interferometer setup. The acoustic stimulus consisted of five simultaneously presented frequencies of equal intensity, which allowed us to estimate the frequency response at the measurement site. The sound intensity was close to the guinea pigs behavioral hearing threshold (40), as we expected the largest effect at low sound intensities. Note that the stated sound pressure levels were not corrected for the effect of immersing the middle ear of the preparation in tissue culture medium, which reduced the effective stimulus level by ~30 dB (41).

Simultaneous acoustic stimulation had no effect on the size and dynamics of the reported position shift. On the other hand, positive current considerably increased the rapidly alternating vibration pattern induced by acoustic stimulation, an effect observed in 20 of the 28 preparations. The spectrum of a representative response reveals maximum vibration amplitude at 200 Hz, the characteristic frequency (CF) expected for this part of the cochlea (Fig. 4 *A*). The asterisks in the panel represent control amplitudes, which were obtained from the part of the record immediately preceding the onset of the positive current step. Note that while positive currents (+17.5 μA, *squares*) increased vibration amplitudes and negative currents (−12.5 μA, *circles*) decreased them, the shape of the curves was similar in all three cases.

Typically, positive current (*squares* in Fig. 4 *B*) increased the vibration amplitudes by 10–12 dB. The largest increase was usually seen below the CF. During negative current injections (*circles* in Fig. 4 *B*), amplitudes at the CF typically decreased by 3 dB. Again, the effect was larger at low frequencies, where reductions as large as 10 dB could be seen. In the entire data set, the largest observed gain at the CF with current injection was 22 dB. These findings demonstrate that positive current injection, which aims to restore the endogenous EP, increased the sound-evoked mechanical response of the outer hearing organ at the Hensen's cells.

Confocal microscopy was used to investigate differences between individual OHC rows. To do so, all preparations were acoustically stimulated with a pure tone around their CF, and the sound-induced vibration trajectories of each OHC during positive and negative current injections were obtained via optical flow ($N_{prep} = 25$; average sound intensity was 86 dB SPL). The trajectories were approximated by a circle that was in one dimension compressed, which allowed a parameterization of the trajectory in a large radius, small radius, and an angle between the large radius and the reticular lamina. The current-induced change of the large radius was significantly different between each OHC row and showed a large increase for OHC row three, a small increase for row two, and small decrease for row one ($p < 0.001$, Fig. 5–$gain_1$). A similar trend could be seen for the small radius, where OHC row three showed a large increase, significantly different from the small increase of row two and the lack of an effect for row one ($p < 0.001$, Fig. 5–$gain_2$). The very same behavior could be observed for the angle between the trajectory and the reticular lamina ($p < 0.01$; Fig. 5, *angle*). Note that in the microscopy experiments the sound pressure level was ~30 dB larger, explaining the small gain that was observed in the confocal imaging data.

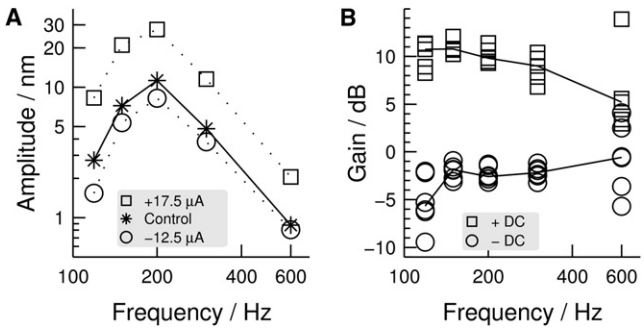

FIGURE 4 Effect of current on sound-induced vibrations of Hensen's cells; interferometric measurements. (*A*) Frequency response of a Hensen's cell during sound (120, 150, 200, 300, 600 Hz each at 54 dB SPL) and direct current simulation, measured with interferometry. Control values were obtained from the first 8 to 50 ms of each measurement trace, before current injection (onset effects <1 dB). (*B*) Frequency dependent gain of the vibration amplitudes due to current injections. Data were acquired during alternating positive (*squares*: +27.5, +22.5, +17.5, +17.5, +17.5 μA) and negative (*circles*: −30, −22.5, −15, −12.5, −25, −12.5 μA) current injections in 30 min.

Role of somatic electromotility

As mentioned, OHCs are capable of fast mechanical force generation. To establish a causal chain between the current injections in scala media and the described static position shift and changes in the vibration patterns, we blocked somatic electromotility with sodium salicylate in 12 preparations (42–44). Fig. 6 *A* gives an example of position shifts evoked by quasistatic current injection and the vibration

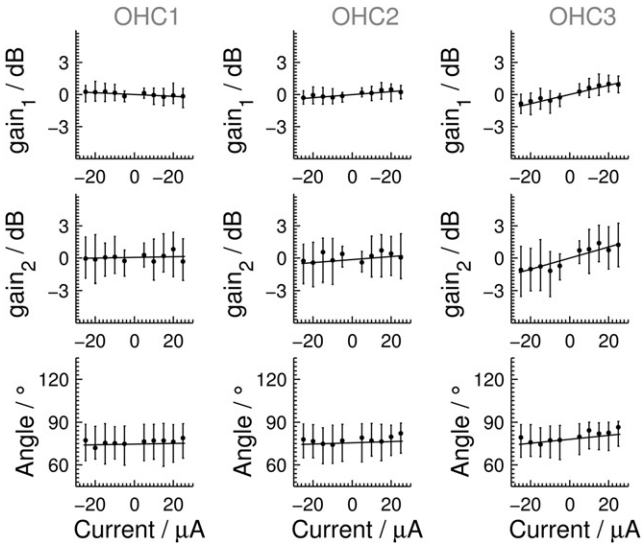

FIGURE 5 Effect of current on sound-induced cochlear vibrations for each OHC row; microscopy measurements. Error bars indicate the 25% and the 75% quartile; data were pooled from 25 experiments with an average sound intensity of 86 dB SPL. Cochlear vibration trajectories can be approximated by a compressed circle with a large and a small radius. $Gain_1$ and $gain_2$ illustrate the gain of the vibration trajectory large and small radius, respectively. Note that the reference value for the gain computation is defined as the mean radius of the smallest current stimulation of each experimental trial. The angle between the major radius of the vibration trajectory and the reticular lamina is shown in the last row.

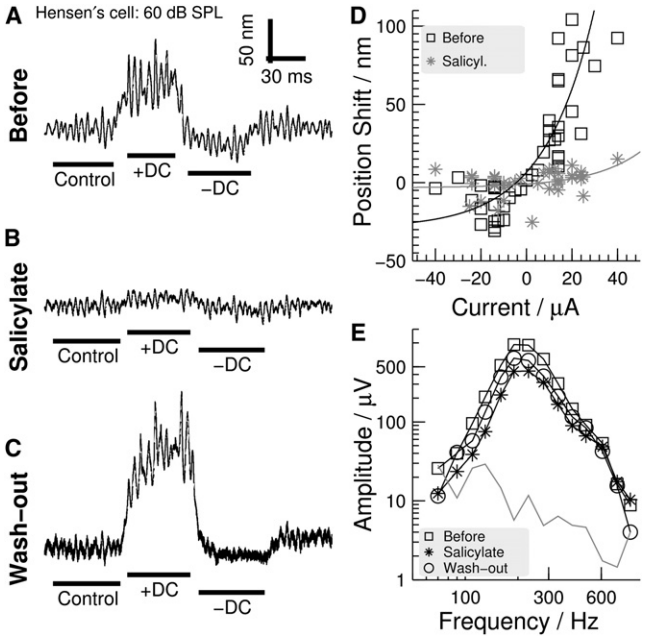

FIGURE 6 Effect of salicylate; interferometry measurements. (*A–C*) Vibration patterns during sound (170, 200, 250, 350, and 650 Hz each at 60 dB SPL) and direct current stimulation (± 14 μA): (*A*) at the start of the experiment, (*B*) during salicylate application, and (*C*) after washout of salicylate. (*D*) Position shift amplitude as function of applied direct current; data were pooled from nine experiments at comparable experimental time points. Solid lines indicate the models used for statistical analysis: $F[x] = c_1\exp[c_2x] - c_1$, where for "Before": $c_1 = 30$ nm; $c_2 = -0.05$ μA^{-1}; and for "Salicylate": $c_1 = 2$ nm; $c_2 = -0.05$ μA^{-1}. Note that c_2 originated from Fig. 1 *C* and was held constant. (*E*) Frequency response of the microphonic potential in the absence of current stimulation. Gray curve shows the measured microphonic potential outside of scala media (10 μm from penetration site) directly after the experiment. It is almost identical to the noise floor, indicating a high impedance of Reissner's membrane.

pattern resulting from simultaneous acoustic stimulation. In this example, positive and negative current was delivered in the same record at the time intervals indicated by the horizontal bars below the trace. Note that these data were obtained early in the experiment, when the effects of current were less than maximal, because the endogenous EP had not yet decayed fully. After 15 min of perfusion of scala tympani with 10 mM sodium salicylate, neither negative nor positive current injections could elicit substantial position shifts (see Fig. 6 *B* and Fig. 6 *D* shows pooled data from nine preparations). This effect was significant ($p < 0.001$) and fully reversible; 30 min after eliminating salicylate from the perfusion system, current injections again caused position shifts (Fig. 6 *C*). Note that during salicylate treatment, current injections also had little effect on sound-induced vibration amplitudes. These data strongly suggest that the observed position shift and alteration of the vibration pattern requires somatic electromotility.

To verify that the observed effect of salicylate was due to the inhibition of somatic electromotility, we monitored the sound-evoked microphonic potential. This is an alternating current potential resulting from the amplitude modulated MET current flowing into the hair cells. Substantial alterations in the mechanical properties of the organ of Corti, or in the transduction process itself, would lead to alterations in microphonic potentials. In the absence of current injection, the frequency response of the microphonic potential decreased by 4 dB during salicylate treatment and partially recovered after washout (Fig. 6 *E*). Similar observations were made for the control amplitudes of the sound-evoked motion with a less potent recovery. The small reversible reduction during salicylate treatment can be attributed to the fact that even when the endogenous EP has vanished, an electrical gradient remains between scala media and the negative membrane potential of the OHCs. Neither a CF shift nor a broadening of the frequency response of the microphonic potential or sound-evoked vibration could be observed during salicylate treatment. These data suggest that MET and the passive mechanics of the hearing organ are both unaffected by salicylate treatment.

Role of MET channel

OHCs are spatially and electrically isolated from scala media, except for their apical surfaces where the hair bundles are located. It is reasonable to expect that the current injections into scala media change the size of the current passing through the MET channels. To test this hypothesis, MET channels were blocked with the fluorescent dye FM1-43 (45), which was injected into scala media through the microelectrode. The spatial extent of the block was therefore limited to the surroundings of the electrode tip and a washout was not possible (see Fig. 7 *C*). Before FM1-43 application, position shifts were clearly noticeable with current injection (Fig. 7 *A*). After introducing FM1-43 into scala media, the same current induced a smaller position shift (Fig. 7 *B*; $N_{prep} = 6$) and no change in sound-evoked vibration amplitudes could be observed during current injections. The channel blockers d-tubocurarine (46) ($N_{prep} = 6$) and streptomycin (47,48) ($N_{prep} = 3$) were also used, with similar results to FM1-43. Composite measurements of position shifts before and during MET blocker application are illustrated in Fig. 7 *D* for a range of positive and negative current injections. The position shift amplitude decreased significantly during the blocking of MET channels ($p < 0.001$). There was no appreciable difference between the compounds used for blocking the MET channels. Note that the remaining position shift could be mediated by unblocked MET channels or another ion channel type in the apical membrane of the OHCs (i.e., the purinergic P2X channel in the stereocilia (49)).

As expected, blocking the MET channel reduced microphonic potentials substantially, as illustrated for FM1-43 (Fig. 7 *E*). The reduction was frequency specific and largest at the CF. This can be explained by the highest FM1-43

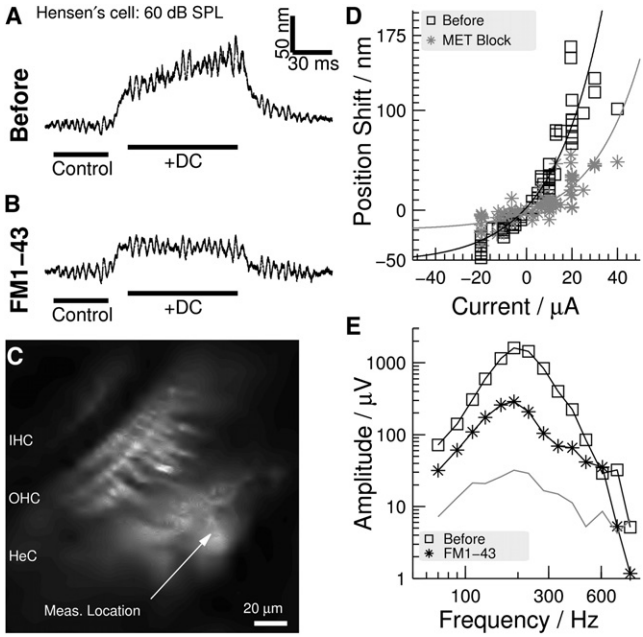

FIGURE 7 Role of the MET channel; interferometry measurements. (*A*) Vibration patterns during sound (170, 200, 250, 350, 650 Hz each at 60 dB SPL) and direct current stimulation (+20 μA): (*A*) at the start of the experiment; (*B*) during FM1-43 application. (*C*) Wavelet denoised confocal image after FM1-43 application shows bright labeling of the OHCs near the electrode. (*D*) Position shift amplitude as function of applied current before and during the blocking of MET channels with FM1-43, d-tubocurarine, or streptomycin; data were pooled from 15 experiments at comparable experimental time points. Solid lines indicate the models used for statistical analysis: $F[x] = c_1\exp[c_2x] - c_1$, where for "Before": $c_1 = 55$ nm; $c_2 = -0.05\ \mu A^{-1}$; and for "MET block": $c_1 = 17$ nm; $c_2 = -0.05\ \mu A^{-1}$. Note that c_2 originated from Fig. 1 *C* and was held constant. (*E*) Frequency response of the microphonic potential in the absence of current stimulation. Gray curve shows the microphonic potential outside of scala media (10 μm from penetration site) directly after experiment.

concentration near the electrode tip, as supported by imaging, which showed a diminishing fluorescence with increasing distance from the electrode (Fig. 7 *C*). Thus, contributions from hair cells distant to the site of the measured microphonic potential were less effected than contributions near the electrode, leading to a broadening of the frequency response of the microphonic potential (Fig. 7 *E*).

DISCUSSION

We have shown that a positive polarization of scala media leads to a sustained electromotile response of the OHCs. This response modifies the organ of Corti geometry and changes the sound-evoked cochlear vibrations drastically. Interfering with the MET channel or with somatic electromotility nearly abolishes both the static position shifts and the modulation of cochlear vibrations.

The in vitro preparation of the guinea pig temporal bone enables us to study sensory transduction in the intact organ of Corti. A hallmark of transduction, the cochlear microphonic potential is similar in our preparation to in vivo measurements both in amplitude and in tuning (50). This testifies that the opening in the cochlear apex, which acts as a shunt for the sound-induced pressure oscillations, does not greatly affect the cochlear vibration pattern at the measurement location. The apical opening also reduces the hydrostatic pressure that the perfusion puts on the basilar membrane (51).

In the intact hearing organ, the apex and the base of the OHCs are connected to different supporting cells. These supporting cells do not just apply the appropriate mechanical load to the OHCs but also have a potential regulatory function (52,53). The second important function of the structure supporting the OHCs is to maintain the physical and electrical barrier separating scala media and the fluid surrounding the OHC body. This maintains the hair bundle and hair cell body in very different surroundings and at very different potentials, a situation that cannot presently be mimicked in isolated cell experiments.

Positive polarization of scala media leads to depolarization of the OHC basolateral wall and a shortening of the OHC soma. Even though this is true for all three rows of OHCs, the resulting position shift of the reticular lamina is very different for OHC row one and two and OHC row three. The inner part of the reticular lamina close to OHC row one and two moves toward scala tympani, whereas at OHC row three and at the Hensen's cells the reticular lamina moves toward scala vestibuli. The difference likely arises from the very different attachment points of each row of OHCs to the organ of Corti. Therefore, each row of OHCs will experience different mechanical loads and motion constraints. Similar row dependent position shifts have been observed in isolated cochlear turns of the gerbil (19), supporting the presented radial component of the reticular lamina position shift and the position shift of the OHC row three soma.

The sustained deformation of the reticular lamina during positive current injections into scala media will also result in shearing between the tectorial membrane and the reticular lamina. This will likely deflect the hair bundles of each OHC row in the excitatory direction, thereby increasing the open probability of MET channels. The positive polarization of scala media will also increase the electrical gradient across the MET channel. Both effects give rise to a positive feedback loop, as they increase OHC depolarization, which leads to further deformation of the reticular lamina. A limitation of the feedback loop is necessary to avoid extreme position shifts and to keep the organ of Corti in a state where it can respond to acoustic stimulation. The final position therefore reflects interactions between the scala media polarization, hair cell polarization, the mechanical impedance of the organ of Corti (54), and fast and slow adaptation (55). However, we could not see any kind of adaptation occurring on a timescale of a few milliseconds to hundreds of milliseconds, which suggest that the mechanical impedance is the main limiting factor.

It has been known for a long time that electrical current applied across the organ of Corti can alter cochlear function. The application of an alternating current leads to oscillatory deformations of the organ in vitro and to acoustic emissions in vivo, even though the cochlear vibration pattern is somewhat different when evoked by acoustic and electrical stimulation (18–20,56). On the other hand, forcing a quasistatic current across the organ of Corti alters distortion product otoacoustic emissions in vivo (16). The exact mechanisms by which the EP modifies cochlear function are still unclear, especially in the speech-encoding, apical region of the cochlea that was examined here (26–28). Static electromotile activity in the absence of sound can modify the physical parameters of the hearing organ, such as stiffness (57) and tension (17), which will influence sound-evoked vibration patterns. However, the effect on the vibration pattern is significantly different for various cochlear structures. The inner part of the reticular lamina, close to OHC row one, displayed a decrease of the sound-evoked vibrations during positive polarization of scala media, whereas the vibrations increased for the outer part. At the level of the Hensen's cells the interferometer data showed a maximum motion increase of 22 dB, whereas the gains reported at high frequencies can be 40 dB and more (26). Although this is merely a quantitative difference, it is known that high-frequency amplification is also accompanied by sharpening of the frequency response (58) and a shift of the vibration pattern toward the apex (59). Both effects are largely lacking in our data even though we do observe some frequency-dependent gain (Fig. 4 *B*). These differences between apical and basal cochlear amplification are corroborated by auditory nerve and psychophysical data (60,61). Finally, positive feedback emerges as a unifying characteristic of cochlear amplification at both low and high frequencies, but the underlying mechanisms may still harbor significant differences in various cochlear regions.

SUPPORTING MATERIAL

A figure and a movie are available at http://www.biophysj.org/biophysj/supplemental/S0006-3495(11)00558-3.

Author contributions: data acquisition, S.J. and M.P.; analysis, S.J.; manuscript preparation, S.J., A.F., and M.P.; study design, A.F. and S.J.

The authors thank Dr. Anna Magnusson, Heike Hevekerl, and Prof. Mats Ulfendahl for their support and constructive criticism.

This study was supported by the Wallenberg Foundations, the Swedish Research Council K2011-63X-14061-11-3, Tysta Skolan Foundation, Hörselskadades Riksförbund, and the funds of Karolinska Institutet.

REFERENCES

1. Harris, G. G., L. S. Frishkopf, and Å. Flock. 1970. Receptor potentials from hair cells of the lateral line. *Science.* 167:76–79.
2. Russell, I. J., G. P. Richardson, and A. R. Cody. 1986. Mechanosensitivity of mammalian auditory hair cells in vitro. *Nature.* 321:517–519.
3. Corey, D. P., and A. J. Hudspeth. 1983. Kinetics of the receptor current in bullfrog saccular hair cells. *J. Neurosci.* 3:962–976.
4. Hudspeth, A. J., and D. P. Corey. 1977. Sensitivity, polarity, and conductance change in the response of vertebrate hair cells to controlled mechanical stimuli. *Proc. Natl. Acad. Sci. USA.* 74:2407–2411.
5. Davis, H. 1965. A model for transducer action in the cochlea. *Cold Spring Harb. Symp. Quant. Biol.* 30:181–190.
6. Zidanic, M., and W. E. Brownell. 1990. Fine structure of the intracochlear potential field. I. The silent current. *Biophys. J.* 57:1253–1268.
7. Sewell, W. F. 1984. The relation between the endocochlear potential and spontaneous activity in auditory nerve fibres of the cat. *J. Physiol.* 347:685–696.
8. Spoendlin, H. 1969. Innervation patterns in the organ of corti of the cat. *Acta Otolaryngol.* 67:239–254.
9. Kennedy, H. J., M. G. Evans, …, R. Fettiplace. 2006. Depolarization of cochlear outer hair cells evokes active hair bundle motion by two mechanisms. *J. Neurosci.* 26:2757–2766.
10. Ashmore, J. F. 1987. A fast motile response in guinea-pig outer hair cells: the cellular basis of the cochlear amplifier. *J. Physiol.* 388:323–347.
11. Brownell, W. E., C. R. Bader, …, Y. de Ribaupierre. 1985. Evoked mechanical responses of isolated cochlear outer hair cells. *Science.* 227:194–196.
12. He, D. Z. Z., and P. Dallos. 1999. Somatic stiffness of cochlear outer hair cells is voltage-dependent. *Proc. Natl. Acad. Sci. USA.* 96:8223–8228.
13. Zheng, J., W. Shen, …, P. Dallos. 2000. Prestin is the motor protein of cochlear outer hair cells. *Nature.* 405:149–155.
14. Santos-Sacchi, J., and J. P. Dilger. 1988. Whole cell currents and mechanical responses of isolated outer hair cells. *Hear. Res.* 35: 143–150.
15. Yu, N., M. L. Zhu, and H. B. Zhao. 2006. Prestin is expressed on the whole outer hair cell basolateral surface. *Brain Res.* 1095:51–58.
16. Mountain, D. C. 1980. Changes in endolymphatic potential and crossed olivocochlear bundle stimulation alter cochlear mechanics. *Science.* 210:71–72.
17. Mammano, F., and J. F. Ashmore. 1993. Reverse transduction measured in the isolated cochlea by laser Michelson interferometry. *Nature.* 365:838–841.
18. Chan, D. K., and A. J. Hudspeth. 2005. Mechanical responses of the organ of corti to acoustic and electrical stimulation in vitro. *Biophys. J.* 89:4382–4395.
19. Karavitaki, K. D., and D. C. Mountain. 2007. Imaging electrically evoked micromechanical motion within the organ of corti of the excised gerbil cochlea. *Biophys. J.* 92:3294–3316.
20. Hubbard, A. E., and D. C. Mountain. 1983. Alternating current delivered into the scala media alters sound pressure at the eardrum. *Science.* 222:510–512.
21. Dallos, P. 1992. The active cochlea. *J. Neurosci.* 12:4575–4585.
22. Fridberger, A., and J. B. de Monvel. 2003. Sound-induced differential motion within the hearing organ. *Nat. Neurosci.* 6:446–448.
23. Jacob, S., C. Johansson, …, A. Fridberger. 2009. A digital heterodyne laser interferometer for studying cochlear mechanics. *J. Neurosci. Methods.* 179:271–277.
24. Fridberger, A., I. Tomo, …, J. Boutet de Monvel. 2006. Imaging hair cell transduction at the speed of sound: dynamic behavior of mammalian stereocilia. *Proc. Natl. Acad. Sci. USA.* 103:1918–1923.
25. Jacob, S., I. Tomo, …, M. Ulfendahl. 2007. Rapid confocal imaging for measuring sound-induced motion of the hearing organ in the apical region. *J. Biomed. Opt.* 12:021005.
26. Cooper, N. P., and W. S. Rhode. 1997. Mechanical responses to two-tone distortion products in the apical and basal turns of the mammalian cochlea. *J. Neurophysiol.* 78:261–270.

27. Zinn, C., H. Maier, …, A. W. Gummer. 2000. Evidence for active, nonlinear, negative feedback in the vibration response of the apical region of the in-vivo guinea-pig cochlea. *Hear. Res.* 142:159–183.

28. Khanna, S. M., and L. F. Hao. 2000. Amplification in the apical turn of the cochlea with negative feedback. *Hear. Res.* 149:55–76.

29. Conlee, J. W., and M. L. Bennett. 1993. Turn-specific differences in the endocochlear potential between albino and pigmented guinea pigs. *Hear. Res.* 65:141–150.

30. Melichar, I., and J. Syka. 1987. Electrophysiological measurements of the stria vascularis potentials in vivo. *Hear. Res.* 25:35–43.

31. Gafni, M., and H. Sohmer. 1976. Intermediate endocochlear potential levels induced by hypoxia. *Acta Otolaryngol.* 82:354–358.

32. Nuttall, A. L., and M. Lawrence. 1980. Endocochlear potential and scala media oxygen tension during partial anoxia. *Am. J. Otolaryngol.* 1:147–153.

33. Maier, H., C. Zinn, …, A. W. Gummer. 1997. Development of a narrow water-immersion objective for laser interferometric and electrophysiological applications in cell biology. *J. Neurosci. Methods.* 77:31–41.

34. Flock, Å., E. Scarfone, and M. Ulfendahl. 1998. Vital staining of the hearing organ: visualization of cellular structure with confocal microscopy. *Neuroscience.* 83:215–228.

35. Fridberger, A., J. Widengren, and J. Boutet de Monvel. 2004. Measuring hearing organ vibration patterns with confocal microscopy and optical flow. *Biophys. J.* 86:535–543.

36. R Development Core Team. 2011. R: A Language and Environment for Statistical Computing. R Foundation for Statistical Computing, Vienna, Austria.

37. Fridberger, A., J. Boutet de Monvel, and M. Ulfendahl. 2002. Internal shearing within the hearing organ evoked by basilar membrane motion. *J. Neurosci.* 22:9850–9857.

38. Tomo, I., J. Boutet de Monvel, and A. Fridberger. 2007. Sound-evoked radial strain in the hearing organ. *Biophys. J.* 93:3279–3284.

39. Marcon, S., and R. Patuzzi. 2008. Changes in cochlear responses in guinea pig with changes in perilymphatic K+. Part I: summating potentials, compound action potentials and DPOAEs. *Hear. Res.* 237:76–89.

40. Hood, L. J., C. I. Berlin, …, E. K. Barlow. 1991. Objective auditory threshold estimation using sine-wave derived responses. *Hear. Res.* 55:109–116.

41. Brundin, L., Å. Flock, …, M. Ulfendahl. 1992. The tuned displacement response of the hearing organ is generated by the outer hair cells. *Neuroscience.* 49:607–616.

42. Kakehata, S., and J. Santos-Sacchi. 1996. Effects of salicylate and lanthanides on outer hair cell motility and associated gating charge. *J. Neurosci.* 16:4881–4889.

43. Shehata, W. E., W. E. Brownell, and R. Dieler. 1991. Effects of salicylate on shape, electromotility and membrane characteristics of isolated outer hair cells from guinea pig cochlea. *Acta Otolaryngol.* 111:707–718.

44. Tunstall, M. J., J. E. Gale, and J. F. Ashmore. 1995. Action of salicylate on membrane capacitance of outer hair cells from the guinea-pig cochlea. *J. Physiol.* 485:739–752.

45. Gale, J. E., W. Marcotti, …, G. P. Richardson. 2001. FM1-43 dye behaves as a permeant blocker of the hair-cell mechanotransducer channel. *J. Neurosci.* 21:7013–7025.

46. Glowatzki, E., J. P. Ruppersberg, …, A. Rüsch. 1997. Mechanically and ATP-induced currents of mouse outer hair cells are independent and differentially blocked by d-tubocurarine. *Neuropharmacology.* 36:1269–1275.

47. Ohmori, H. 1985. Mechano-electrical transduction currents in isolated vestibular hair cells of the chick. *J. Physiol.* 359:189–217.

48. Wang, X., S. Jia, …, D. Z. He. 2007. Streptomycin and gentamicin have no immediate effect on outer hair cell electromotility. *Hear. Res.* 234:52–58.

49. Housley, G. D. 1998. Extracellular nucleotide signaling in the inner ear. *Mol. Neurobiol.* 16:21–48.

50. Honrubia, V., and P. H. Ward. 1968. Longitudinal distribution of the cochlear microphonics inside the cochlear duct (guinea pig). *J. Acoust. Soc. Am.* 44:951–958.

51. Fridberger, A., J. T. van Maarseveen, …, Å. Flock. 1997. Pressure-induced basilar membrane position shifts and the stimulus-evoked potentials in the low-frequency region of the guinea pig cochlea. *Acta Physiol. Scand.* 161:239–252.

52. Yu, N., and H. B. Zhao. 2009. Modulation of outer hair cell electromotility by cochlear supporting cells and gap junctions. *PLoS ONE.* 4:e7923.

53. Flock, Å., B. Flock, …, M. Ulfendahl. 1999. Supporting cells contribute to control of hearing sensitivity. *J. Neurosci.* 19:4498–4507.

54. Scherer, M. P., and A. W. Gummer. 2004. Impedance analysis of the organ of corti with magnetically actuated probes. *Biophys. J.* 87:1378–1391.

55. Eatock, R. A. 2000. Adaptation in hair cells. *Annu. Rev. Neurosci.* 23:285–314.

56. Nowotny, M., and A. W. Gummer. 2006. Nanomechanics of the subtectorial space caused by electromechanics of cochlear outer hair cells. *Proc. Natl. Acad. Sci. USA.* 103:2120–2125.

57. He, D. Z. Z., S. Jia, and P. Dallos. 2003. Prestin and the dynamic stiffness of cochlear outer hair cells. *J. Neurosci.* 23:9089–9096.

58. Ruggero, M. A., and N. C. Rich. 1991. Furosemide alters organ of corti mechanics: evidence for feedback of outer hair cells upon the basilar membrane. *J. Neurosci.* 11:1057–1067.

59. Ren, T. 2002. Longitudinal pattern of basilar membrane vibration in the sensitive cochlea. *Proc. Natl. Acad. Sci. USA.* 99:17101–17106.

60. Vinay, and, B. C., and Moore. 2008. Effects of activation of the efferent system on psychophysical tuning curves as a function of signal frequency. *Hear. Res.* 240:93–101.

61. van der Heijden, M., and P. X. Joris. 2006. Panoramic measurements of the apex of the cochlea. *J. Neurosci.* 26:11462–11473.